

Atomic structure of conducting nanofilaments in TiO₂ resistive switching memory

Deok-Hwang Kwon¹, Kyung Min Kim^{1,2}, Jae Hyuck Jang¹, Jong Myeong Jeon¹, Min Hwan Lee^{1,2}, Gun Hwan Kim^{1,2}, Xiang-Shu Li³, Gyeong-Su Park³, Bora Lee⁴, Seungwu Han¹, Miyoung Kim^{1*} and Cheol Seong Hwang^{1,2*}

Resistance switching in metal oxides could form the basis for next-generation non-volatile memory. It has been argued that the current in the high-conductivity state of several technologically relevant oxide materials flows through localized filaments, but these filaments have been characterized only indirectly, limiting our understanding of the switching mechanism. Here, we use high-resolution transmission electron microscopy to probe directly the nanofilaments in a Pt/TiO₂/Pt system during resistive switching. *In situ* current–voltage and low-temperature (~130 K) conductivity measurements confirm that switching occurs by the formation and disruption of Ti_nO_{2n-1} (or so-called Magnéli phase) filaments. Knowledge of the composition, structure and dimensions of these filaments will provide a foundation for unravelling the full mechanism of resistance switching in oxide thin films, and help guide research into the stability and scalability of such films for applications.

Innovations in modern information technology are critically dependent on the development of denser, faster and less energy-consuming non-volatile memory (NVM)¹. Charge-based memories, such as dynamic random access memory (DRAM) and flash memory, will suffer from performance degradation as the scaling limit is approached². The development of non-charge-based memory is therefore essential for extending Moore's law over the few next decades. Among the many contenders for next-generation NVM based on a non-charge mechanism, resistance-switching random access memory (RRAM) has attracted increasing attention because of the advantages in its fabrication process as well as its outstanding device performance³⁻⁶. In addition, RRAM is also suitable for the three-dimensional stacking of memory layers, which can lead to the ultimate high-density memory⁷.

RRAM is based on the reversible dielectric (soft) breakdown of an insulator, particularly metal oxides. From a microscopic point of view, resistance switching in various materials can be classified broadly into two different mechanisms^{3,8}. In the valence-change mechanism, the creation and electromigration of oxygen vacancies induces the distribution of the carrier density and the valence states of cations. For example, it is convincingly demonstrated in ref. 9 that the oxygen vacancies in SrTiO₃ migrate through the dislocation network and affect the conductivity. The device driven by this mechanism usually shows bipolar behaviour, in which the conducting and insulating states are switched with opposite bias polarity. In the fuse–antifuse mechanism, in which the interplay between the thermal effect and the redox reaction in the filament and its vicinity has a crucial role, metallic filaments are created through the insulator matrix during the electroforming process, and are fused as a result of Joule heating and the electric field¹⁰⁻¹⁴. In the antifuse process, the Joule heating-assisted reduction reconnects the filament. In this case, resistance switching can be achieved with only one bias polarity, and is thus termed unipolar switching behaviour. Among the various oxide materials demonstrating

unipolar switching behaviour^{5,10-12,15-19}, TiO₂ appears to be one of the most promising switching materials to use this switching mechanism^{5,10-12,15,16}. Several materials also show both types of switching behaviours²⁰⁻²².

In both valence-change and fuse–antifuse mechanisms, many aspects of the switching behaviour can be understood by assuming that the current flows through localized filaments in the conducting state^{11,13,16}. However, basic information about the conducting filaments, such as their composition, size and density, has been inferred only indirectly^{23,24}. Consequently, it is very difficult to understand the resistance-switching phenomena in terms of detailed chemical processes. The low density of metallic filaments poses a significant hurdle to characterizing their physical properties¹⁰. In this study, extensive and careful high-resolution transmission electron microscopy (HRTEM) and electron diffraction analyses have shown that the conducting filaments in TiO₂ are composed of Ti_nO_{2n-1} (mostly $n = 4$ or 5), known as Magnéli phases. *In situ* local current–voltage (I - V) measurements in TEM indicate that this transformed structure can indeed constitute an electrical conduction path. The conductivity measurements at low temperature (~130 K) and *in situ* switching experiments confirm that the overall resistance switching was induced by the Magnéli phase filaments.

Electrical switching behaviour

Three types of TiO₂ films were examined: pristine, SET and RESET samples. The pristine sample was prepared using plasma-enhanced atomic layer deposition of 40-nm-thick TiO₂ thin films followed by the deposition of a platinum electrode, as shown in Fig. 1a (see Methods). To switch the pristine metal–insulator–metal (MIM) sample to the conducting state (forming process), a negative bias is applied to the top electrode with an appropriate compliance current (Fig. 1b). The TiO₂ film in this low-resistance state is called the 'SET' sample. The scanning electron microscopy (SEM) image in Fig. 1c shows that a part of the platinum top electrode is

¹Department of Materials Science and Engineering, Seoul National University, Seoul 151-744, Korea, ²Inter-university Semiconductor Research Center, Seoul National University, Seoul 151-744, Korea, ³Analytical Research Laboratory, Samsung Advanced Institute of Technology, PO Box 111, Suwon 440-600, Korea, ⁴Department of Physics, Ewha Womans University, Seoul 120-750, Korea. *e-mail: mkim@snu.ac.kr; cheolsh@snu.ac.kr

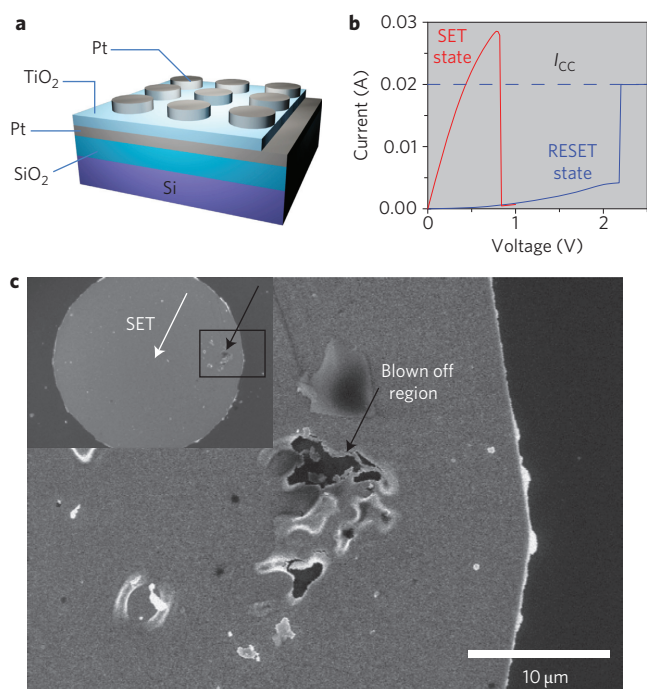


Figure 1 | Schematic of the device structures and SEM image after the forming process. **a**, Schematic of the Pt/TiO₂/Pt stack. **b**, Typical *I*-*V* curves of the MIM sample showing three different conduction states. **c**, SEM image of the top electrode in the SET state. The image shows the blown-off region marked as the black box in the low-magnification SEM image in the inset.

blown off after the forming process, as indicated by the black arrow. The small explosion is probably caused by the sudden evolution of compressed excess oxygen gas¹⁶. The blown-off region of the sample may correspond to a location where the strongest filaments have developed, and was useful for identifying the filaments at the initial stage of the present work (Supplementary Fig. S1). However, this part does not act as a current path in the following switching process, because the top electrode is missing. Two of the capacitor structures were electroformed in this manner. A negative bias was further applied to one of the two electroformed structures to switch the sample into a high-resistance state. The TiO₂ film in this high-resistance state is called the 'RESET' sample. Details regarding resistance switching by means of the *I*-*V* sweeps are reported in ref. 11.

HRTEM observation

The electron diffraction (ED) patterns and fast Fourier transformed (FFT) micrographs of the HRTEM images from each sample were examined extensively to determine the crystallographic structure of the filaments and the remaining part of the TiO₂ films. In the case of the pristine TiO₂ sample, the majority phase was identified as a meta-stable brookite structure (Supplementary Fig. S2), rather than a rutile or anatase structure. This is understandable, because the deposition conditions of the pristine sample were far from the thermodynamic stability condition, even with plasma application at a growth temperature of 250 °C. It is also noted that nanoscale non-stoichiometric TiO_{*x*} (*x* < 2) phases were pervasive throughout the thin films, determined by the FFT of local regions of a few nanometres, although their volume ratio is relatively small.

The ED patterns from the SET and RESET samples, however, have features clearly distinguishable from pristine TiO₂. First, a substantial amount of the dielectric films was changed, in both cases, into the rutile or anatase phases. Thermal heating during the *I*-*V* sweeps might have triggered the transition to more stable phases. Second, ED spots with smaller scattering angles than those of the anatase

[101] spots appear. Because the anatase [101] spots, corresponding to a *d*-spacing of 0.351 nm, have the smallest observable diffraction angle in the ED patterns from stoichiometric TiO₂ with the brookite, anatase and rutile structures, those extra diffraction spots are indicative of the presence of non-stoichiometric Ti_{*n*}O_{2*n*-1} (mostly *n* = 4 or 5). (Possible diffraction spots that can be excited by multiple scattering, both from the same grain and from separate grains, were carefully traced and were not considered for further examination.) This is known as a Magnéli phase²⁵. The Magnéli phase is a defective structure derived from the ideal rutile phase, and can be described by the two-dimensional rutile (121) slabs made from octahedral TiO₆ with an *n*-layer thickness in the direction normal to the slab plane. The adjacent two slabs were displaced by 1/2[011] to accommodate the oxygen deficiencies²⁵. Therefore, the *n*th (121) plane constitutes an antiphase boundary, which is known as the crystallographic shear plane. It is also well known that most of these Magnéli phases are metallic conductors near room temperature²⁶. Therefore, the presence of a Magnéli phase in the SET and RESET samples could be responsible for the observed resistance-switching behaviours.

Most Magnéli structures, whether connected or disconnected in the HRTEM images, were fairly straight in both SET and RESET samples. This implies that most nanofilaments are normal to the electrode; if the filaments deviate significantly from the vertical direction, one should be able to observe an image of slant nanofilaments in HRTEM. This is reasonable, because the nanofilaments are likely to be formed along the direction of applied electric fields, which is the normal direction to the film surface in the planar MIM geometry.

In the following, a more detailed analysis of ED patterns for SET samples is presented. Figure 2a, for the SET state, shows a clear and conical pillar with diameters of ~15 and 3 nm at the cathode (TE) and anode (BE) interfaces, respectively, comprising a Magnéli phase. The microscopic structure was confirmed from an ED pattern in Fig. 2b, which shows the diffraction spot with a *d*-spacing of 0.62 nm (marked with a circle). This was identified as the (002) spot of a Magnéli phase with *n* = 4. The dark-field image from this spot is displayed in Fig. 2c. The high-resolution image of the bright area in the dark-field image is shown in Fig. 2a. The FFT image in Fig. 2d also confirms that the structure is Ti₄O₇. The diffraction image in Fig. 2e is the simulated [140] diffraction pattern of Ti₄O₇, which coincides well with the FFT image. Another image for the connected filament in the SET sample can be found in Supplementary Fig. S3.

An extensive examination of the SET samples revealed only six connected filament images in five 10-μm-wide focused ion beam (FIB) samples. (This includes two strong filaments found within the blown-off region.) Considering the low probability of the thin TEM specimen containing nanofilaments and the information limit of TEM, this does not necessarily mean that there are only six conducting filaments in such a large area of the sample. In addition, the observation of the nanofilaments in TEM requires that the filaments must be in specific crystallographic orientations for the given electron-beam directions.

Besides the nanofilaments in the connected shape, several disconnected nanofilaments in Magnéli phases were also found. (In fact, most of the nanofilaments were disconnected.) This can be understood based on the nanofilament growth process. During the electroforming step, many nanofilaments may start to grow. As the nanofilaments connect the top and bottom electrodes, large currents would flow through these metallic paths. The bias voltage is largely reduced when the current level reaches the compliance limit, preventing further growth of other nanofilaments. Figure 2f shows a typical partial filament. (The images in Fig. 2f-j correspond to the images in Fig. 2a-e, respectively.) Most of the incomplete Ti₄O₇ or Ti₅O₉ pillars were present near the top electrode. This means that the nanofilaments usually grow from the cathode. In addition, these pillars typically have conical shapes, with a wider diameter at the cathode side. (In the connected nanofilaments,

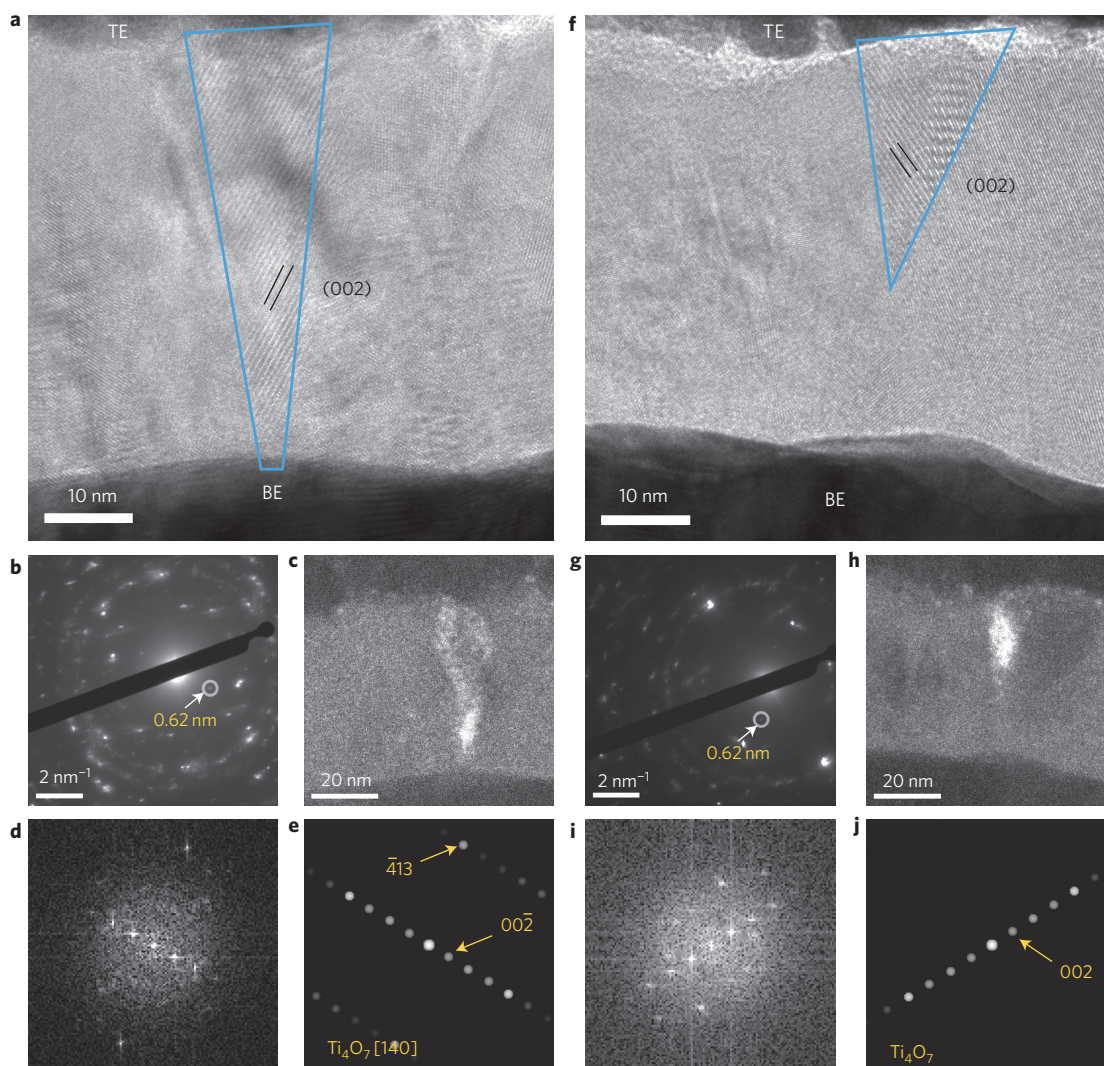


Figure 2 | Magnéli structures in the SET sample. **a–e**, High-resolution TEM image of a Ti_4O_7 nanofilament (**a**), selected-area diffraction pattern of the film (**b**), dark-field image obtained from the diffraction spot marked as a circle in the diffraction pattern (**c**), a fast Fourier transformed micrograph of the high-resolution image of Ti_4O_7 (**d**), and the corresponding simulated diffraction pattern (**e**). The Bloch-wave method was used to simulate the diffraction patterns. **f–j**, Disconnected Ti_4O_7 structure in the conical shape. The images are presented in the same manner as for the connected filament in **a–e**.

three of the observed filaments have conical shapes; see Fig. 2a, Fig. 5c and Supplementary Fig. S3.) These findings are consistent with a filament-growth model for TiO_2 as already proposed^{11,15}.

TEM analysis of the RESET samples indicates that they are similar to SET samples, except that no connected nanofilament could be found. In the RESET operation, the connected nanofilament should be ruptured, possibly by thermally assisted electromigration of oxygen ions^{10,11,15}. However, disconnected nanofilaments would not be affected by the RESET operation. (One of the disconnected nanofilaments found in the RESET sample is shown in Supplementary Fig. S4.)

The observed filament diameters (measured at the middle point along the length) in the SET and RESET states ranged from 5 to 10 nm, with the distance between them being between 0.1 and 5 μm (considering both connected and incomplete filaments). These are essential parameters for estimating the ultimate packing density of the RRAM device. The relatively large distances between filaments are an unfavourable feature of the device, because this can comprise a scaling limit. However, it should be noted that once a filament is established, there would be no further filament formation in the adjacent region, because the current flows mostly through the connected filament. Therefore, even if the device size becomes very small, namely

$\ll 100 \times 100 \text{ nm}^2$, it is anticipated that there would be at least one filament with which resistance switching could occur. In fact, a lower density of filaments could be advantageous for device applications, because once a filament is formed in a nanoscale memory cell, it is unlikely that another will form in the same cell. (Multiple filaments may deteriorate the reproducibility of the resistance switching behaviour.) In this sense, a smaller cell size is conducive to better uniformity and repeatability. Therefore, the size of the filament is a more important parameter. The small size of the filaments suggests that the memory cell size can in principle be scaled down to tens of nanometres.

Even though the Magnéli phase is a metal in the bulk phase, it is unclear whether the nano-sized Magnéli pillar is also conducting. To establish this, the electrical conductivity of the Magnéli nanofilaments in the SET sample was measured using a local *in situ* I - V scan in TEM (Fig. 3a) using the scanning tunnelling microscopy (STM) tip operating in conductive atomic force microscopy (CAFM) mode. The sample was prepared from the region where the top electrode was blown off. Figure 3b shows the I - V curves obtained from the Magnéli structure (red circles) and from the area $\sim 50 \text{ nm}$ away from the filament where the Magnéli structure was not identified (blue squares). The local I - V curve showed an electrical conductivity ratio of $\sim 1,000$ between the two locations. It was noted that the

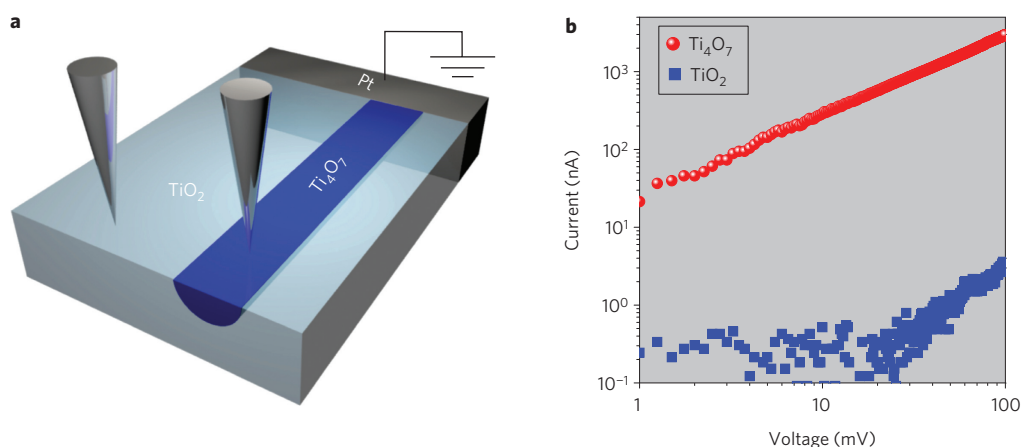


Figure 3 | In situ I - V scan on nanofilaments. **a**, Schematic to show the experimental set-up. **b**, Local I - V curves measured on the Ti_4O_7 structure (red circles) and on the anatase structure that is ~ 50 nm away from the Ti_4O_7 (blue squares). The conductivity ratio between the two locations is $\sim 1,000$.

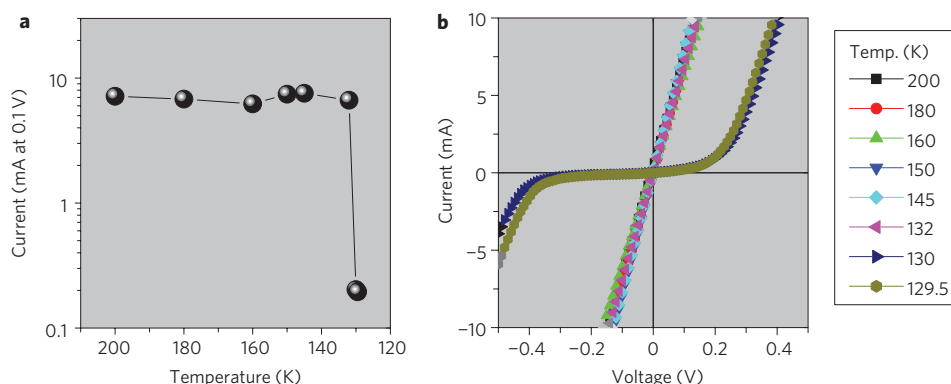


Figure 4 | Temperature-dependent conduction behaviours of the MIM sample in the SET state. **a**, Current values measured at 0.1 V with the temperature varying between 129.5 and 200 K. **b**, Corresponding I - V curves. The I - V curve at 305 K was almost identical to that of 200 K (not shown). It is found that the sample changes its conduction behaviour from metallic (down to 132 K) to semiconducting (or insulating) at 130 and 129.5 K.

current variation due to the difference in probe pressure on the sample was $\sim 15\%$, and there was a $\sim 10\%$ difference with and without incident high-energy electrons (for the TEM observation). The contact resistance might also complicate measurement of the absolute resistance values. However, the large conductivity ratio suggests that the observed Magnéli phases are indeed localized conducting paths. In passing, it is worth mentioning that there are three orders of difference in the current level between Figs 1b and 3b. This is because a large number of filaments contribute to the total current in the pad-type device in Fig. 1. In contrast, Fig. 3b was obtained for TEM samples in which only one filament was probed.

Low-temperature measurements

Although TEM analysis in the above provided a clear observation of the Magnéli phase filaments, it needs to be further confirmed that the nanofilaments are responsible for the conductivity in the SET state. This is because other parts of the TiO_2 film, which may contain a large portion of oxygen-deficient TiO_x phase (or even metal atoms), may also contribute to electrical conduction^{27,28}. To this end, the temperature-dependent I - V curves of the MIM sample in the SET state were measured. It is known that the Magnéli-structured Ti_4O_7 phase exhibits a metal (high-temperature) to semiconductor (low-temperature) transition at ~ 150 K, with an abrupt drop in electrical conductivity by a factor of $\sim 1,000$, caused by charge ordering of Ti^{3+} and Ti^{4+} ions²⁹. Figure 4a shows the current values of the MIM sample measured at 0.1 V with the temperature varying between 129.5 and 200 K. It is found that the current drops sharply at 130 K. In Fig. 4b, the

corresponding I - V curves indicate that the conduction behaviour changes from metallic to semiconducting (or insulating) near 130 K. (The I - V curve at 305 K was almost identical to that at 200 K.) This is similar to results reported for single-crystal Ti_4O_7 in ref. 29, except for the transition temperature (130 K versus 150 K), and confirms that the electrical conduction in the SET state is governed by the Magnéli nanofilaments. The discrepancy in the transition temperature could be ascribed to different correlation effects between the nanostructure of the Magnéli phase in the matrix of TiO_2 and the single crystal. The I - V measurements at temperatures ranging from 313 to 363 K (data not shown) showed that the on-state resistance increases with the temperature, which confirms metallic conduction in the SET state.

In situ switching in TEM

To further confirm that the observed structure and the accompanying electrical properties of Magnéli phase nanofilaments are manipulated by the applied voltage, an *in situ* RESET operation on a connected Magnéli structure was performed in TEM using the experimental set-up shown in Fig. 5a. The STM tip approached the TE with the BE grounded. The Magnéli structure of the connected nanofilament was confirmed (Fig. 5c) and then the I - V curve of the SET state was obtained (red circles in Fig. 5b). The current density calculated from Fig. 5b reaches $\sim 1 \times 10^6$ A cm^{-2} . Although this current density is not high enough to induce electromigration of atoms in the filament, the accompanying Joule heating effect may thermally anneal the filament. An I - V sweep to a lower voltage (-1.0 V) was then performed to reset the TEM sample. The I - V curve after the RESET operation

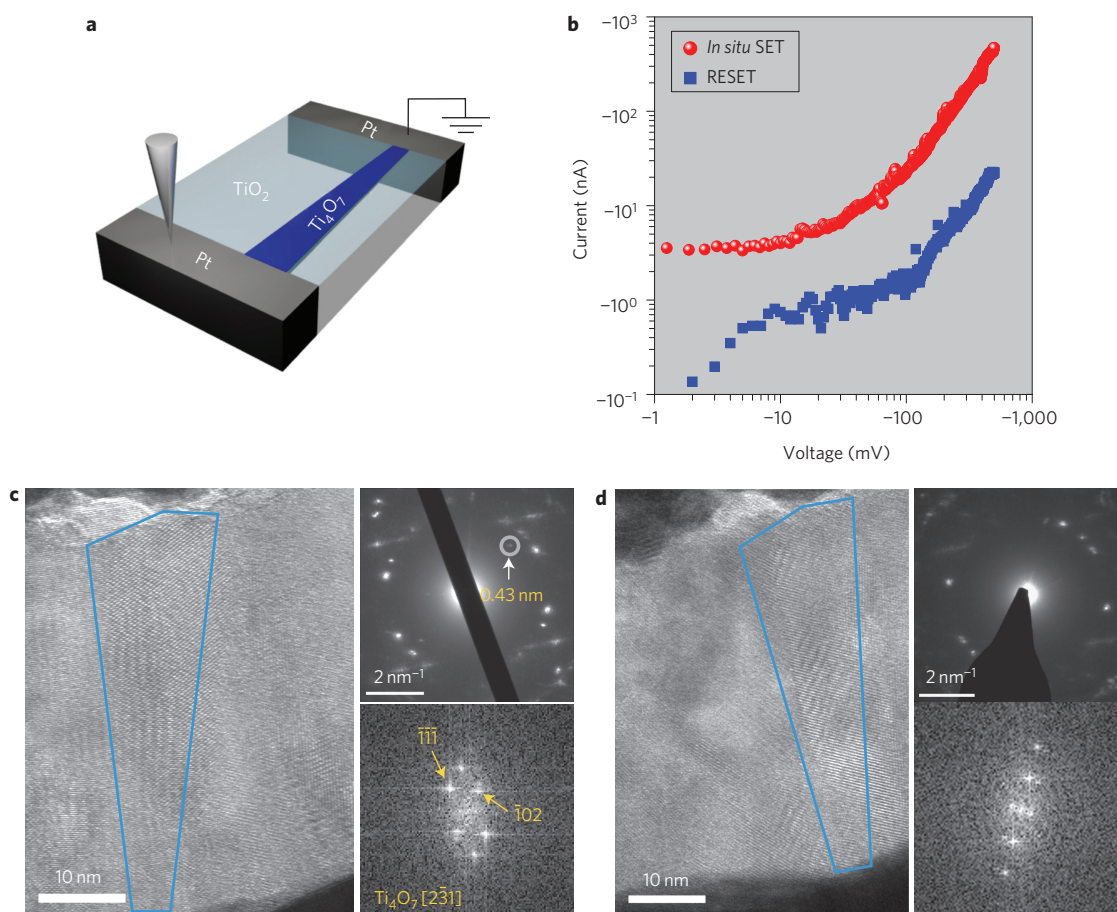


Figure 5 | Structural transformation after an *in situ* RESET experiment. **a**, Schematic to depict the experimental set-up. **b**, Local I - V curves in a log scale before and after RESET. The STM probe approached the top electrode, and the I - V curves represent the electrical conduction between the top and bottom electrodes. **c**, High-resolution image, diffraction pattern and fast Fourier transformed micrograph of the Magnéli structure before RESET. **d**, The corresponding images after RESET. The diffraction spot (marked as a circle in **c**) from the Magnéli structure disappeared after RESET.

represented in Fig. 5b (blue squares) indicates that the conductivity was lowered by a factor of 10–20. Concurrently, the structure of the former Magnéli nanofilament was converted into other structures (probably anatase), as shown in Fig. 5d. The diffraction spots from the Magnéli structure also disappeared as expected. This confirms that the RESET operation corresponds to the phase transformation of nanofilaments from Magnéli to other stoichiometric phases. Because the experiment was performed in a high vacuum condition, it is likely that the oxygen atoms were supplied from the neighbouring oxide phase. In Fig. 5b, the conductivity change in the *in situ* RESET was less pronounced when compared to the pad-type switching in Fig. 1c. From a comparison with Fig. 3b, it is found that the current in the SET state is lower than the corresponding value in Fig. 3b, meaning that this particular filament is less conducting. The two orders of difference in the SET-state currents in Figs 3b and 5b could be attributed to the disparate filament shapes. In Fig. 3b, the filament is straight with a diameter of ~ 10 nm, and the measurement tip is positioned in the middle of the filament. The filament in Fig. 5b is cone-shaped with diameters of 10 (top) and 5 nm (bottom) and the tip is positioned on the electrode. Consideration of these geometric differences can account for one order of difference. In addition to this, the sharp and narrow shape of the filament near the bottom electrode may complicate the transport behaviour at the interface. The non-ohmic behaviour in Fig. 5b might also be caused by this.

The *in situ* SET experiment was also tried and the conductivity significantly increased to a value much higher than that of the initial SET state with the reappearance of the diffraction spots of the Magnéli

phase. However, the connected Magnéli phase was not identified in the TEM observation area. This suggests that the newly formed nanofilament was located in a region outside the area observed by HRTEM. (The observable area by HRTEM was only ~ 50 nm wide, and the diameter of the area contributing to the diffraction patterns was over ~ 1 μm across.) Even though the filament in the present *in situ* experiment was completely eliminated and was not recovered, this does not exclude the possibility of partial rupture of the filament. In fact, from a CAFM study on the TiO_2 film (data not shown), it was often observed that some filaments were recreated at the same spot, suggesting that those filaments were partially broken.

Conclusions

The identification of the Magnéli phase as conducting filaments has important implications for the switching mechanism in RRAM. At the initial stage, a random oxygen vacancy will be created as the oxygen atoms are displaced from the bulk position by the external field and thermal effects. Above a critical density, oxygen vacancies will spontaneously rearrange to form an ordered structure. Indeed, first-principles calculations with the same computational set-up as in ref. 28 found that the Magnéli phase is more stable than the rutile phase with a uniform distribution of oxygen vacancy, by ~ 2 eV per Ti_4O_7 formula unit. Therefore, with increasing concentration of oxygen vacancies, there should be a strong thermodynamic driving force to form the Magnéli phase. The presence of a stable metallic phase explains the outstanding endurance of many RRAM devices, which is difficult to rationalize if the conducting paths

comprise a random distribution of point defects. In this respect, it would be worth reexamining the conducting path in other oxides in terms of vacancy ordering or oxygen-deficient phases. A recent report on the valence reduction of a switching filament in CuO cells is, thus, very interesting³⁰.

Methods

A 40-nm-thick TiO₂ thin film was deposited on a 100-nm-thick sputtered platinum/SiO₂/silicon substrate by plasma-enhanced atomic layer deposition at 250 °C using titanium tetraisopropoxide and plasma-activated O₂ as the precursor and oxygen source, respectively. Structural and chemical characterization using grazing-angle incidence X-ray diffraction and X-ray photoelectron spectroscopy revealed the as-grown TiO₂ film to have an amorphous to polycrystalline mixed anatase and brookite structure with an oxygen/titanium ratio of ~2.1. The grain shape was granular, and no specific preferred crystallographic orientation was observed. A 50-nm-thick circular platinum top electrode with a diameter of 300 μm was then fabricated by electron-beam evaporation followed by a lift-off photolithographic process. The resistive switching behaviour of the MIM structure was measured at room temperature using an HP4145B semiconductor parameter analyser in the *I*-*V* sweep mode. The switching behaviour of the sample was measured by applying a negative bias voltage to the top electrode with the bottom electrode grounded. Two samples were electroformed using the *I*-*V* sweep with a compliance current of 20 mA. One of the two samples was set again to the high-resistance state by applying another reset *I*-*V* sweep. Therefore, SET samples experienced only one *I*-*V* sweep and the RESET samples experienced two *I*-*V* sweeps. To confirm that the observed Magnéli phase filaments governs the overall resistive switching behaviour of the MIM sample, the conductance of the MIM sample in the SET state was measured at low temperature (down to 129.5 K) using a low-temperature stage of the CAFM (JEOL JSPM 5400) in a high-vacuum (1×10^{-6} Torr) condition. A platinum-coated STM-type tip was used to minimize the contact resistance. The presence of intervening SiO₂ below the MIM structure adversely interferes with the fluent heat transfer between the MIM structure and the stage. To mitigate this problem, the TiO₂ film surface was thermally connected to the cold stage surface using silver paste.

The TEM specimens were prepared using a FIB etching technique to include the dielectrics directly under the top platinum electrode. A 300 kV field emission TEM (Jeol 3000F) and a 200 kV field emission TEM (Tecnai F20) were used for electron diffraction, dark-field imaging and HRTEM. *In situ* localized *I*-*V* measurements in Fig. 3 were performed on the Magnéli structures, which were confirmed by ED and HRTEM before *in situ* experiments. A two-terminal *I*-*V* curve was measured using a double-tilt STM (Nanofactory Instruments AB, ST-1000) installed on a TEM holder of Tecnai F20G serving as a manipulator. *I*-*V* was measured in CAFM mode. The contact between the tungsten probe and the TiO₂ sample was made using the STM unit, which could control the probe movement at sub-nanometre resolution with a piezotube. The integrity of the contact was constantly monitored during the *I*-*V* measurement. The TEM specimen for the *in situ* RESET experiment was prepared by FIB from the SET sample, retaining both TE and BE, and negative bias was applied to the TE to keep the electrical bias direction the same as that in pad-type switching. The STM tip approached the TE instead of the TiO₂ film to avoid inevitable specimen damage due to excessive heating related to the high contact resistance between the tip and TiO₂. The connecting area between the top electrode and the TEM copper grid was removed carefully by FIB in order to cut off the current path between the top and bottom electrodes through the copper grid.

Received 6 October 2009; accepted 25 November 2009;
published online 17 January 2010

References

- Burr, G. W. *et al.* Overview of candidate device technologies for storage-class memory. *IBM J. Res. Dev.* **52**, 449–464 (2008).
- Waser, R. (ed.) *Nanoelectronics and Information Technology* Ch. 4 (Wiley-VCH, 2003).
- Waser, R. & Aono, M. Nanoionics-based resistive switching memories. *Nature Mater.* **6**, 833–840 (2007).
- Strukov, D. B., Snider, G. S., Stewart, D. R. & Williams, R. S. The missing memristor found. *Nature* **453**, 80–83 (2008).
- Seo, S. *et al.* Reproducible resistance switching in polycrystalline NiO films. *Appl. Phys. Lett.* **85**, 5655–5657 (2004).
- Meijer, G. I. Who wins the nonvolatile memory race? *Science* **319**, 1625–1626 (2008).
- Likharev, K. K. & Strukov, D. B. Prospects for the development of digital circuits. *Proc. IEEE Int. Symp. Nanoscale Architectures* 109–116, 2007.
- Sawa, A. Resistive switching in transition metal oxides. *Mater. Today* **11**, 28–36 (2008).
- Szot, K., Speier, W., Bihlmayer, G. & Waser, R. Switching the electrical resistance of individual dislocation in single-crystalline SrTiO₃. *Nature Mater.* **5**, 312–320 (2006).
- Choi, B. J. *et al.* Resistive switching mechanism of TiO₂ thin films grown by atomic-layer-deposition. *J. Appl. Phys.* **98**, 033715 (2005).

- Kim, K. M., Choi, B. J., Shin, Y. C., Choi, S. & Hwang, C. S. Anode-interface localized filamentary mechanism in resistive switching of TiO₂ thin films. *Appl. Phys. Lett.* **91**, 012907 (2007).
- Rohde, C. *et al.* Identification of a determining parameter for resistive switching of TiO₂ thin films. *Appl. Phys. Lett.* **86**, 262907 (2005).
- Sato, Y., Kinoshita, K., Aoki, M. & Sugiyama, Y. Consideration of switching mechanism of binary metal oxide resistive junctions using a thermal reaction model. *Appl. Phys. Lett.* **90**, 033503 (2007).
- Russo, U., Ielmini, D., Cagli, C. & Lacaíta, A. L. Self-accelerated thermal dissolution model for reset programming in unipolar resistive-switching memory (RRAM) devices. *IEEE Trans. Electron. Dev.* **56**, 193–200 (2009).
- Kim, K. M. & Hwang, C. S. The conical shape filament growth model in unipolar resistance switching of TiO₂ thin film. *Appl. Phys. Lett.* **94**, 122109 (2009).
- Jeong, D. S., Schroeder, H., Breuer, U. & Waser, R. Characteristic electroforming behaviour in Pt/TiO₂/Pt resistive switching cells depending on atmosphere. *J. Appl. Phys.* **104**, 123716 (2008).
- Shim, H. *et al.* Resistance-switching characteristics of polycrystalline Nb₂O₅ for nonvolatile memory application. *IEEE Electron. Device Lett.* **26**, 292–294 (2005).
- Lee, D. *et al.* Resistance switching of the nonstoichiometric zirconium oxide for nonvolatile memory applications. *IEEE Electron. Device Lett.* **26**, 719–721 (2005).
- Kim, K. M. *et al.* Resistive switching in Pt/Al₂O₃/TiO₂/Ru stacked structures. *Electrochem. Solid State Lett.* **9**, G343–G346 (2006).
- Jeong, D. S., Schroeder, H. & Waser, R. Coexistence of bipolar and unipolar resistive switching behaviors in a Pt/TiO₂/Pt stack. *Electrochem. Solid State Lett.* **10**, G51–G53 (2007).
- Lee, S., Kim, W.-G., Rhee, S.-W. & Yong, K. Resistance switching behaviors of hafnium oxide films grown by MOCVD for nonvolatile memory applications. *J. Electrochem. Soc.* **155**, H92–H96 (2008).
- Yang, Y. C., Pan, F., Liu, Q., Liu, M. & Zeng, F. Fully room-temperature-fabricated nonvolatile resistive memory for ultrafast and high-density memory application. *Nano Lett.* **9**, 1636–1643 (2009).
- Fujiwara, K. *et al.* Resistance switching and formation of a conductive bridge in metal/binary oxide/metal structure for memory devices. *Jpn J. Appl. Phys.* **47**, 6266–6271 (2008).
- Lee, M.-J. *et al.* Electrical manipulation of nanofilaments in transition-metal oxides for resistance-based memory. *Nano Lett.* **9**, 1476–1481 (2009).
- Bursill, L. A. & Hyde, B. G. Crystallographic shear in the higher titanium oxides: structure, texture, mechanisms and thermodynamics. *Prog. Solid State Chem.* **7**, 177–253 (1972).
- Inglis, A. D., Page, Y. L., Strobel, P. & Hurd, C. M. Electrical conductance of crystalline Ti_nO_{2n-1} for *n* = 4–9. *J. Phys. C* **16**, 317–333 (1983).
- Yang, J. J. *et al.* Memristive switching mechanism for metal/oxide/metal nano devices. *Nature Nanotech.* **3**, 429–433 (2008).
- Cho, E. *et al.* First-principles study of point defects in rutile TiO_{2-x}. *Phys. Rev. B* **73**, 193202 (2006).
- Lakkis, S., Schlenker, C., Chakraverty, B. K., Buder, R. & Marezio, M. Metal-insulator transitions in Ti₄O₇ single crystals: crystal characterization, specific heat and electron paramagnetic resonance. *Phys. Rev. B* **14**, 1429–1440 (1976).
- Yasuhara, R. *et al.* Inhomogeneous chemical states in resistance-switching devices with a planar-type Pt/CuO/Pt structure. *Appl. Phys. Lett.* **95**, 012110 (2009).

Acknowledgements

This work was supported by National Research Foundation of Korea grant funded by the Ministry of Education, Science and Technology (2009-0083038) and MEST-AFOSR NBIT Program. C.S.H., K.M.K., M.H.L. and K.H.K. acknowledge support by the National Program for 0.1 Terabit NVM Devices of the Korean Government, the National Research Foundation of Korea (NRF) funded by the Ministry of Education, Science and Technology (grant no. 2009-0081961), and World Class University program through the Korea Science and Engineering Foundation funded by the Ministry of Education, Science and Technology (grant no. R31-2008-000-10075-0). B.L. and S.H. were supported by the Quantum Metamaterials Research Center (grant no. R11-2008-053-03001-0).

Author contributions

D.-H.K., J.H.J. and J.M.J. performed the TEM experiments and analysed the diffraction data. X.-S.L., G.-S.P. and D.-H.K. performed the *in situ* switching experiments in STM-TEM. K.M.K. and G.H.K. fabricated the samples and performed electrical switching experiments. M.H.L. performed the low temperature experiment. B.L. and S.H. performed the first-principles calculation. M.K. and C.S.H. conceived and designed the experiments. M.K., S.H. and C.S.H. co-wrote the paper. All authors discussed the results and commented on the manuscript.

Additional information

The authors declare no competing financial interests. Supplementary information accompanies this paper at www.nature.com/naturenanotechnology. Reprints and permission information is available online at <http://ngp.nature.com/reprintsandpermissions/>. Correspondence and requests for materials should be addressed to M.K. and C.S.H.